

Current Biology

Supplemental Information

**Role of Synchronous Activation  
of Cerebellar Purkinje Cell Ensembles  
in Multi-joint Movement Control**

Tycho M. Hoogland, Jornt R. De Gruijl, Laurens Witter, Cathrin B. Canto, and Chris I. De Zeeuw

Twitches evoked  
by sensory perturbations

Temporal twitch profile

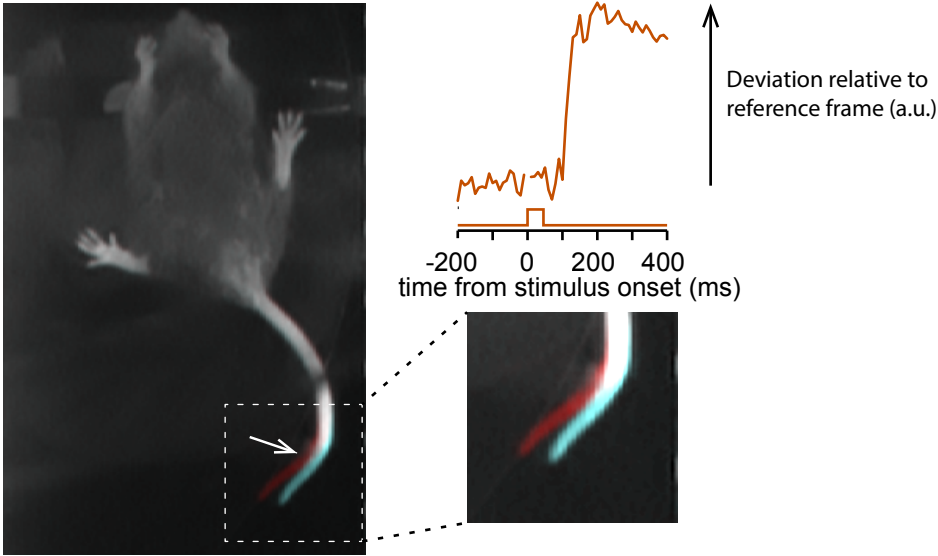


Figure S1

**Figure S1, related to Figure 1. Sensory perturbations evoked using a magnetic clutch along the axis of a disk treadmill**

Brief sensory perturbations could be applied using an electromagnetic coupling device (clutch) along the treadmill axis to which mice responded with brief twitches of limbs and tail (inset and arrow indicating predominant tail twitch in this example). The frame difference in this example was between the frame corresponding to the stimulus offset (cyan) and a frame 130 ms later (red) to show tail displacement. A custom algorithm [S1] was used to generate twitch profiles in response to the sensory perturbation and conveyed information about twitch onset.

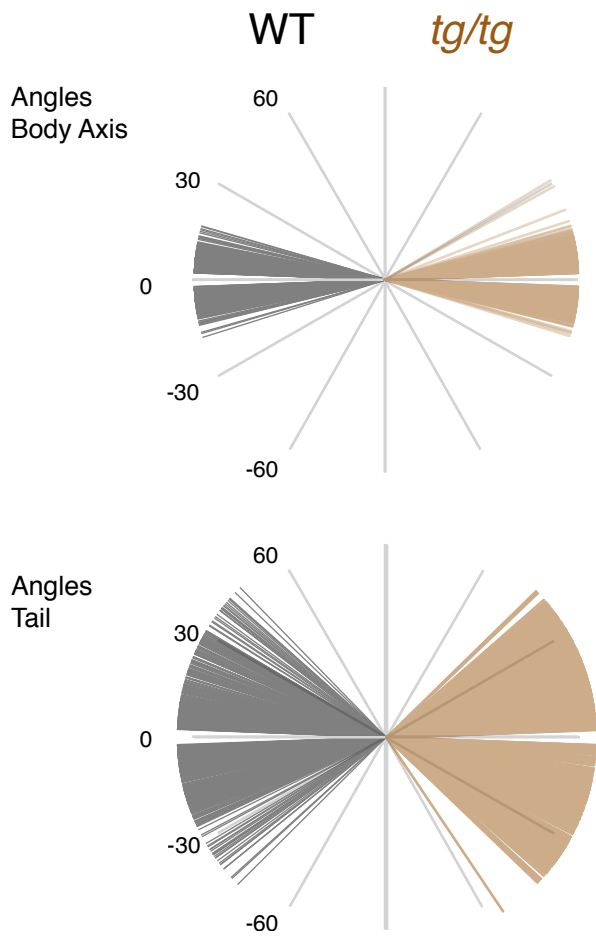


Figure S2

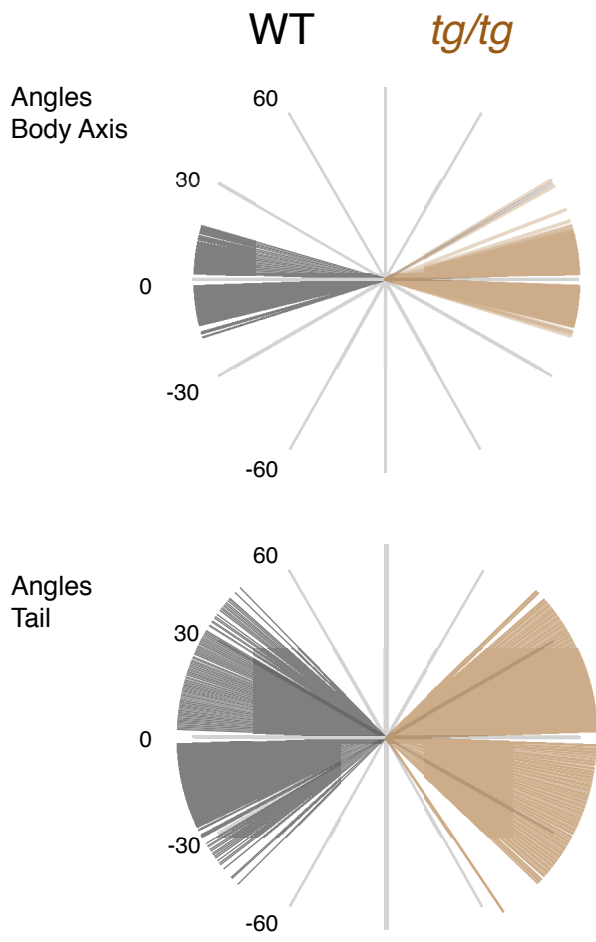


Figure S2

**Figure S2, related to Figure 2. Plot of the body axis and tail angles in wild type and tottering (*tg/tg*) mice during locomotion**

Top: body axis angles for wild type (left) and *tg/tg* mice (right). Bottom: tail axis angles for wild type (left) and *tg/tg* mice (right).

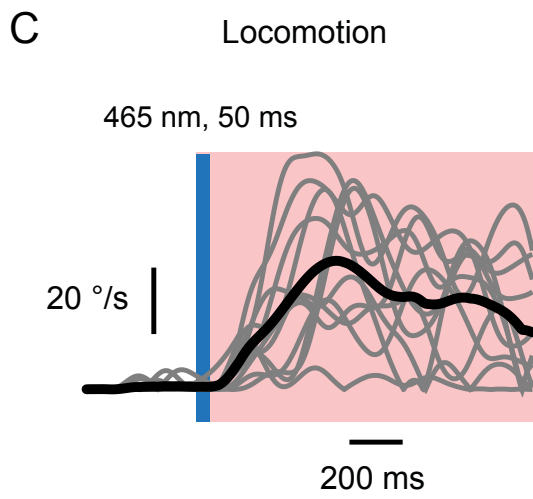
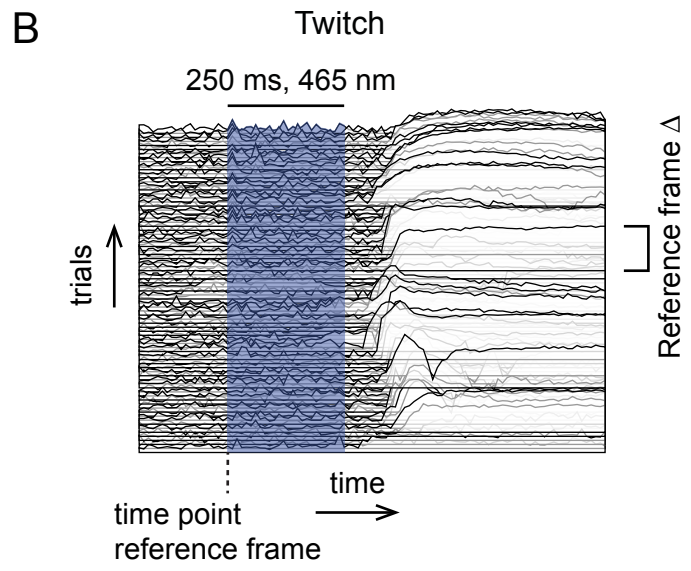
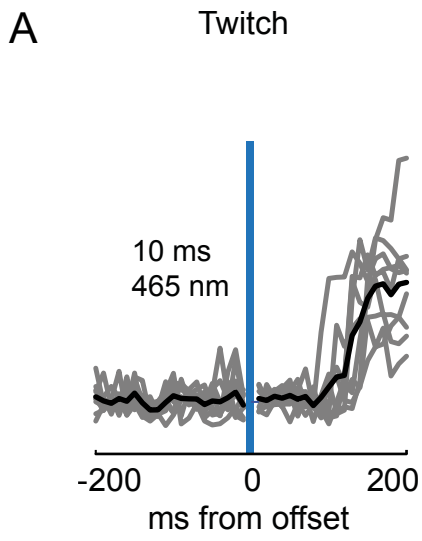


Figure S3

**Figure S3, related to Figure 3. Timing of twitches evoked by optogenetic activation of Purkinje cells**

(A) Optogenetic activation of PCs for durations as short as 10 ms were sufficient to trigger a behavioral response comprising twitches. Shown are individual responses within a single experiment (gray) and the population average (black). (B) Temporal profiles of twitch responses following a 250 ms duration stimulus demonstrating that optogenetic activation of PCs during rest can evoke twitch responses that follow the offset of a light stimulus.



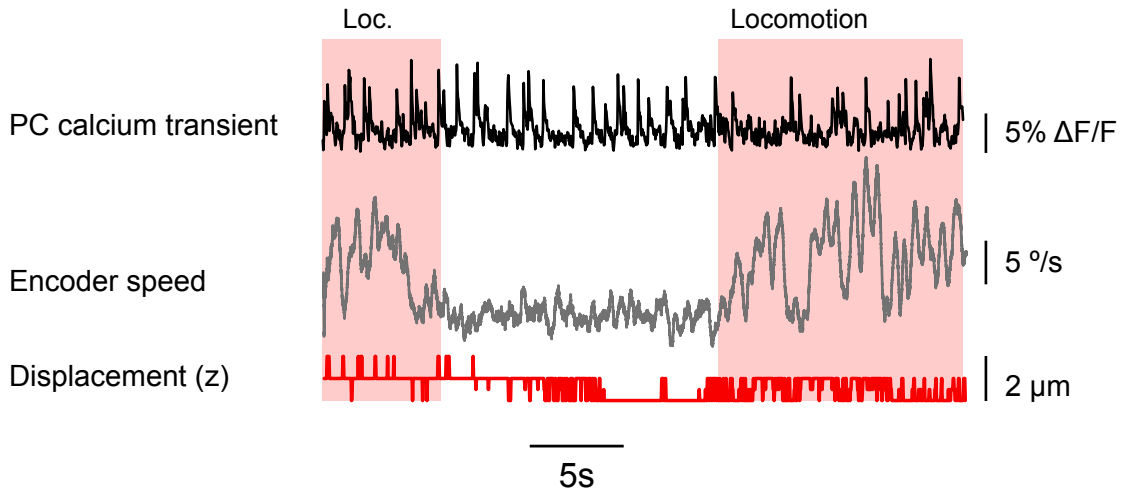


Figure S4

**Figure S4, related to Experimental Procedures. Axial movement during two-photon imaging on a disk treadmill**

Shown are calcium transients recorded from a Purkinje cell (PC), disk encoder speed and axial displacement. Axial displacement was calculated by acquiring a z-stack of images at 1 $\mu$ m intervals when an animal was at rest. Frames obtained during locomotion from a single optical plane were cross-correlated with the reference images at different depths obtained at rest to calculate displacement.

**Table S1. Stance and swing durations in wild type and tottering mice.**

	WT stance (mean±sd)	<i>tg/tg</i> stance (mean±sd)	WT swing (mean±sd)	<i>tg/tg</i> swing (mean±sd)
LF	304±113 ms	325±115 ms	200±69 ms	246±106 ms
RF	277±149 ms	263±125 ms	222±88 ms	265±85 ms
LH	313±147 ms	286±186 ms	208±117 ms	214±96 ms
RH	320±165 ms	282±156 ms	221±71 ms	262±126 ms
	WT vs. <i>tg/tg</i> stance (Kruskal-Wallis): p=0.06		WT vs. <i>tg/tg</i> swing (Kruskal-Wallis): p=1.3*10 <sup>-11</sup>	
	WT stance vs. swing (Kruskal-Wallis): p=1.9*10 <sup>-62</sup>		<i>tg/tg</i> stance vs. swing (Kruskal-Wallis): p=5.6*10 <sup>-11</sup>	

**Table S2. Properties of complex spike elicited calcium transients in PC dendrites of wild type and tottering mice.**

	WT (mean±sd), median	<i>Tg/tg</i> (mean±sd), median	P-value	Type of test
Amplitude $\Delta F/F$ %	6.5±2.6, 6.2 (7354 transients)	4.7±1.5, 4.5 (2624 transients)	$p=2.7*10^{-234}$	K-S, 2-sample
$t_{1/2}$ (ms)	112.3±38.7, 106.7 (7354 transients)	100.1±37.5, 94.0 (2624 transients)	$p=6.5*10^{-52}$	K-S, 2-sample
Rates rest	1.13±0.4, 1.17 (630 dendrites)	1.26±0.4, 1.23 (192 dendrites)	P=0.001	K-S, 2-sample
Rates locomotion	1.43±0.3Hz, 1.40Hz (630 dendrites)	1.52±0.3Hz, 1.55Hz (192 dendrites)	$p=7.9*10^{-07}$	K-S, 2-sample

## Supplemental Experimental Procedures

### Two-photon microscopy

A two-photon microscope (TrimScope II, Lavis BioTec, Bielefeld, Germany) was used in combination with a Chameleon Ultra II pulsed infrared laser (pulse width: 140 fs, repetition rate: 80 MHz; Coherent, Santa Ana, California) to image microcircuits in the cerebellum. All imaging was performed using a 20x, 1.0 N.A. objective (XLUMPLSLN, Olympus, Tokyo, Japan). Images were acquired with sample times of 15 ms and 30 ms per frame. A hyperacuity algorithm was applied to detect CS events triggered off of sensory perturbations, or locomotion onsets to realign events with ms precision [S2]. Imaging was done in the molecular layer of the mouse cerebellum (50-100  $\mu\text{m}$  depth) where CFs trigger CS-mediated calcium transients in PC dendrites. PC CSs were imaged using the synthetic fluorescent calcium indicator Oregon Green BAPTA-1/AM (Life Technologies, Carlsbad, California), which was bolus-loaded into the cerebellar cortex [S3]. Recordings began at least 30 minutes after loading. CS-mediated calcium transients were extracted from PCs in two steps. A median filter with 3 by 3 pixel kernel was applied to all two-photon image frames prior to spatial independent component analysis with the resulting spatial components being used to segment responding PC dendrites [S4]. A threshold consisting of the mean pixel intensity plus five standard deviations was applied to each component. Overlapping pixels were removed and small objects below a size threshold ( $< 15$  pixels) discarded. Fluorescence was averaged over all the pixels contained within each segmented PC dendrite.  $\Delta F/F$  was calculated as described previously [S3].

Calcium transients were high-pass filtered to remove slow baseline fluctuations. Subsequently CS event extraction was performed using a spike train inference algorithm [S5].

### **Optogenetics**

The PC specific PCP2-Cre driver line (The Jackson Laboratory, Maine, JAX # 004146) was crossed with ChR2(H134R)-eYFP mice (Madisen et al., 2012, JAX # 012569). Expression of the L7-ChR2(H134R)-eYFP fusion protein. Craniotomies were made above vermis lobule V. A 400  $\mu\text{m}$  multimode optical fiber (Thorlabs, New Jersey) was placed just above the surface of the cerebellum and secured with Kwik-Sil (World Precision Instruments, Sarasota, Florida) and dental cement (Super-Bond C&B, Sun-Medical, Moriyama City, Japan). A custom LED driver was used to control the output power of the LED [S1]. In our experiments we used 1-3 mW output power as measured coming out of the fiber tip. For the fiber used this corresponded with  $\sim 8-4 \text{ mW/mm}^2$  (1 mW, from surface to Purkinje cell layer) to  $\sim 24-13 \text{ mW/mm}^2$  (3 mW, from surface to Purkinje cell layer) and has been shown using whole-cell recordings in vivo to increase SS firing rate in PCs [S1].

### **Behavioral tracking**

The Matlab code used for the gait tracking analysis, determination of body/tail axis angles and calculation of temporal twitch profiles has been deposited at: <https://github.com/CCCgroup/Tracking>. Whole body twitches evoked by sensory perturbations through engagement of the magnetic clutch were analyzed using a custom algorithm described before in detail [S1].

## **Analysis of gait**

The objects in our monochrome camera data change position, size and shape. Since mice were head-fixed in the setup, standard algorithms for freely moving animals could not be used, as these generally assume constant locations for limbs during stance. Standard blob tracking algorithms for objects moving through frames often use parameters such as size and shape to track targets. In order to detect limb movements and locomotion, we developed a gait tracking application in Matlab (MathWorks, Natick, Massachusetts). As a pre-processing step all frames were denoised using the software CANDLE [S6]. Subsequently, background subtraction was performed on all frames to facilitate object detection. Changes in pixel values between frames were calculated by taking the sum of the absolute value of a subtraction of two consecutive frames. The second frame of pairs of subsequent frames of which the pixel difference values exceeded a threshold of the mean plus one standard deviation were selected to generate a background image. A pixel intensity threshold for object detection as well as a minimum object size criterion were set manually. Thresholded objects were matched between frames, based on the in-frame center-of-mass coordinates and the number of pixels constituting the object. If the distance between the centers of mass exceeded a set threshold (20 pixels,  $\sim 7$  mm) or if the number of pixels changed more than 10% from one frame to the next, a putative match was deemed invalid. If multiple objects were eligible for matching, the closest (Euclidian distance) match was selected. This processing stage generated a set of object trace snippets in which objects were not yet classified, but already temporally linked for a limited sequence of

frames. For object classification, a feed-forward three-layer neural network was used (Neural Network Toolbox) and a training set was generated by taking a selection of 15% of the frames (with a minimum of 150 and a maximum of 500 that always included those frames that were used for rendering the background image and were supplemented with randomly selected frames). The frames used for generating the background image were explicitly included, as these images likely represent the most problematic cases for a trained classifier if such cases were not sufficiently represented in the data set it was trained on. The objects detected in the training set were manually assigned to any of six classes: tail, left hind limb (LH), right hind paw (RH), left front paw (LF), right front paw (RF) and unclassified. The results of this classification were extended to the trace snippets and the neural network was trained on the data, using the following parameters: object size, center-of-mass coordinates, and orientation. The trained network was used to perform a final classification on the entire data set. Following this automated classification, the results were manually inspected and incorrectly classified objects were removed on a frame-by-frame basis. Paw objects moving in the direction of the disk as judged by the magnetic encoder signal were considered as being “in stance”. If the direction of a paw object’s motion ran counter to that of the disc, it was considered to be “in swing”. From the final object set several gait parameters were extracted including stride length and duration.



## Supplemental References

- S1 Witter, L., Canto, C. B., Hoogland, T. M., de Gruijl, J. R., and De Zeeuw, C. I. (2013). Strength and timing of motor responses mediated by rebound firing in the cerebellar nuclei after Purkinje cell activation. *Front. Neural Circuits* 7, 133, 1–14.
- S2 De Gruijl, J. R., Hoogland, T. M., and De Zeeuw, C. I. (2014). Behavioral correlates of complex spike synchrony in cerebellar microzones. *J. Neurosci.* 34, 8937–47.
- S3 Ozden, I., Dombeck, D. A., Hoogland, T. M., Tank, D. W., and Wang, S. S.-H. (2012). Widespread state-dependent shifts in cerebellar activity in locomoting mice. *PLoS One* 7, e42650.
- S4 Hyvärinen, a (1999). Fast and robust fixed-point algorithms for independent component analysis. *IEEE Trans. Neural Netw.* 10, 626–34.
- S5 Vogelstein, J. T., Packer, A. M., Machado, T. a, Sippy, T., Babadi, B., Yuste, R., and Paninski, L. (2010). Fast nonnegative deconvolution for spike train inference from population calcium imaging. *J. Neurophysiol.* 104, 3691–704.
- S6 Coupé, P., Munz, M., Manjón, J. V, Ruthazer, E. S., and Louis, D. (2012). A CANDLE for a deeper in vivo insight. *Med. Image Anal.* 16, 849–864.

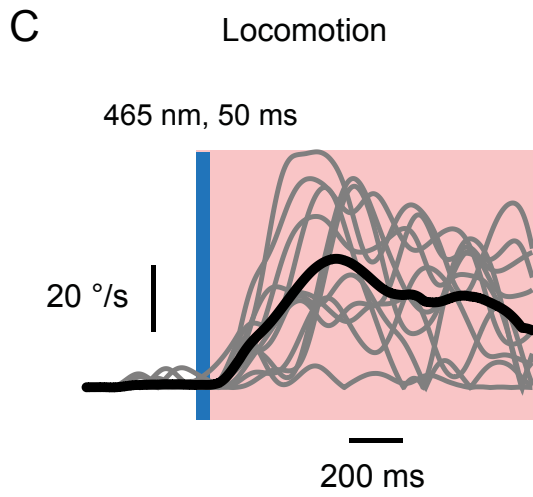
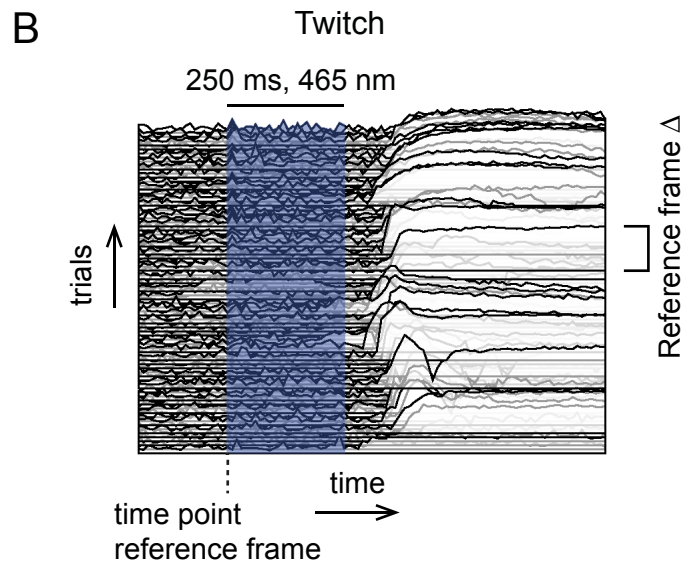
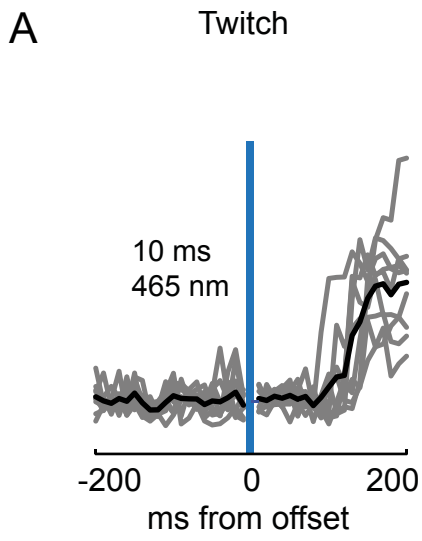


Figure S3

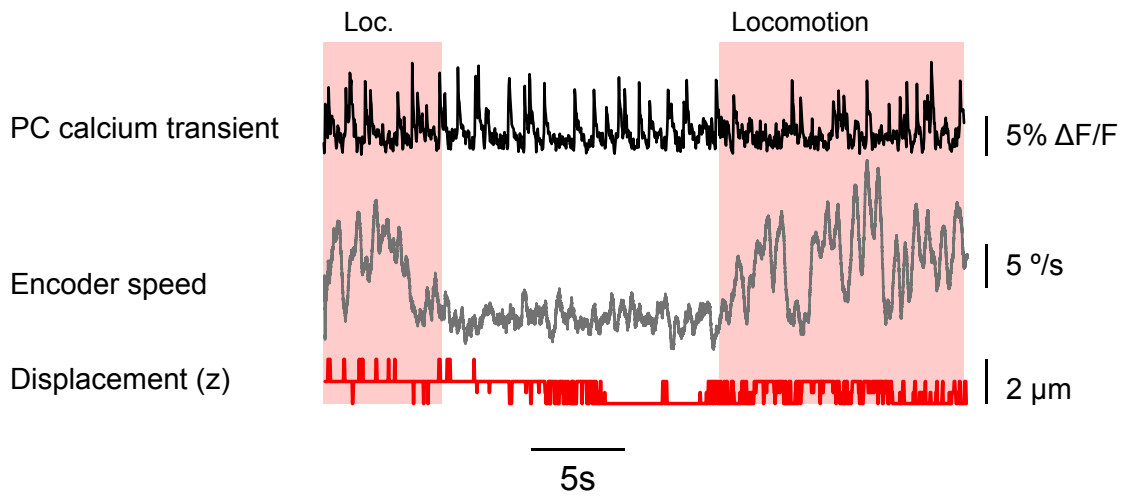


Figure S4